Communications in Physics, Vol. 35, No. 4 (2025), pp. 365-378
DOI: https://doi.org/10.15625/0868-3166/22650

Correlation between current-assisted transversal anisotropy adjustment and magnetoimpedance enhancement in Fe-based microwires

D. H. Hoang[1], **N. V. Tuan**[2], **H. A. Tam**[1], **N. K. Binh**[1], **P. M. Vuong**[1], **H. S. Hong**[3], **V. D. Lam**[4], **L. V. Lich**[5] **and D. T. Huong Giang**[1,†]

[1]*Faculty of Physics Engineering and Nanotechnology, VNU University of Engineering and Technology, Vietnam National University, Hanoi, Vietnam*

[2]*Department of Physics, Le Quy Don Technical University, Hanoi, Vietnam*

[3]*School of Electrical and Electronic Engineering, Hanoi University of Science and Technology*

[4]*Graduate University of Science and Technology, Vietnam Academy of Science and Technology, Hanoi, Vietnam*

[5]*School of Materials Science and Engineering, Hanoi University of Science and Technology, Hanoi, Vietnam*

E-mail: [†]giangdth@vnu.edu.vn

Received 3 April 2025; *Accepted for publication 11 September 2025*; *Published 9 December 2025*

Abstract. *This study investigates the correlation between direct current (DC)-assisted adjustments to transversal magnetic anisotropy and enhancements in the magnetoimpedance (MI) effect in straight microwires fabricated from amorphous Fe-based ribbons. Using a combination of wet chemical etching and laser ablation, microwires with dimensions of approximately 80 μm width and 9 mm length were prepared and characterized via vibrating sample magnetometry, vector network analysis, and infrared thermal imaging. Micromagnetic simulations with MuMax*^{3} *software complemented the experiments to elucidate underlying magnetization dynamics. Results reveal that applying DC bias currents induces a circumferential magnetic field, promoting transversal magnetization and competing with shape anisotropy. In magnetoimpedance characterizations, without bias current, the maximum MI ratio reached 10.1% at a magnetic field orientation of* $\varphi = 45^\circ$ *relative to the microwire axis, compared to 4.8% at* $\varphi = 0^\circ$ *and minimal response at* $\varphi = 90^\circ$*.Introducing a 30 mA bias current enhanced the MI ratio by a factor of 1.3 at* $\varphi = 0^\circ$ *(to 6.15%) and to 13.5% at* $\varphi = 45^\circ$*, with the peak MI field shifting from 60 Oe to 35 Oe. This corresponded to a 3°C temperature rise due to Joule heating, contributing nearly 35% to the MI increase. MI sensitivity peaked at 0.72 %/Oe for* $\varphi = 45^\circ$ *at 30 mA, before declining with higher currents. These findings, supported by simulations showing increased transverse magnetization near the surface, demonstrate how current-induced anisotropy optimizes MI performance, paving the way for advanced, high-sensitivity magnetic sensors in applications like biomedical diagnostics and industrial monitoring.*

Keywords: magnetization; magnetoimpedance; soft magnetic materials; magnetic properties.
Classification numbers: 75.30.Gw; 75.47.-m; 75.50.Kj.

1. Introduction

The rapid advancement of science and technology has driven widespread adoption of intelligent automatic control systems, which in turn has fueled significant interest in sensor technologies, particularly those based on magnetic sensing principles. Among the diverse classes of magnetic sensors, with each optimized for specific measurement ranges, sensitivities, resolutions, and operational modalities, the magnetoimpedance (MI) effect-based sensors have garnered considerable attention due to their outstanding features, including high sensitivity, excellent resolution, and wide operational bandwidth [1–3]. The MI effect is defined as the variation of the electrical impedance of a magnetic conductor when subjected to an external magnetic field [4]. Originally discovered in the 1930s [5, 6], this phenomenon has since become a focal point for research, with extensive efforts devoted to understanding, optimizing, and commercializing MI-based devices.

The core of the MI effect lies the skin depth phenomenon [7], whereby alternating current (AC) induces a frequency-dependent penetration depth of electromagnetic fields in the conductor. Variations in external magnetic fields alter the transverse magnetic permeability of the material, which in turn modulates the skin depth and consequently the overall impedance of the conductor. Enhancing the MI response has therefore become a primary objective in sensor development, achieved through systematic optimization of multiple parameters including material composition and microstructure, fabrication processes (e.g., heat treatments, deposition techniques), device geometry (shape and dimensions), operational conditions (frequency, current amplitude, temperature), and auxiliary stimuli such as applied direct current (DC) or mechanical stress [2, 3, 8, 9]. Notably, applying DC bias currents can induce reconfiguration of vortex-like magnetic domain structures surrounding the conductor, effectively amplifying the MI response [10, 11].

Among magnetic materials, amorphous alloys have emerged as superior candidates for MI sensor applications owing to their inherently soft magnetic characteristics and enhanced ductility. These properties are rooted in their liquid-like atomic arrangement, which lacks long-range crystalline order and thereby suppresses magnetocrystalline anisotropy. In particular, FeCSi-based amorphous alloys exhibit exceptional magnetic softness, low coercivity, linear magnetic responses, high permeability, and high Curie temperature of 1000 K, significantly exceeding that of ferrites and permalloys [3, 8, 12]. These characteristics enable extraordinarily high sensitivity and fast response to external magnetic fields, surpassing many conventional crystalline or alloyed counterparts. Furthermore, their unique atomic disorder fosters reduced magnetic losses, making FeCSi alloys ideal for developing ultra-sensitive, miniaturized MI sensors with superior performance in diverse fields such as biomedical diagnostics, security, and industrial monitoring.

Despite these advancements, prior studies have predominantly focused on either isolated experimental characterizations [13, 14] or theoretical modeling [10, 15–18] without fully integrating these approaches into a comprehensive framework that combines simulation, experimental validation, and performance evaluation. To address this gap, the present study provides a systematic investigation of MI behavior in straight micro-scale conductors fabricated from amorphous soft magnetic FeCSi ribbons. Specifically, this work (i) examines the influence of key external parameters, including magnetic field orientation and strength, electrical current amplitude, and Joule

heating effects on the MI response, and (ii) employs micromagnetic simulations to elucidate the fundamental physical mechanisms driving these phenomena. By bridging experimental insights and computational modeling, this research advances the understanding of MI sensor behavior and informs the design of optimized devices. The outcomes of this study lay the groundwork for practical implementations of MI-based magnetic field sensors and contribute to the development of highly sensitive, robust devices tailored for diverse real-world scenarios.

2. Methodology

2.1. Sample preparation

Prior to sensor characterization and subsequent correlation with micromagnetic simulations aimed at elucidating the underlying physical mechanisms, the microwires were fabricated through a combination of wet chemical etching and laser ablation techniques. The overall fabrication process, starting from a continuous FeCSi ribbon, is schematically illustrated in Fig. 1. Initially, a commercially available amorphous FeCSi ribbon, 20 μm in thickness, was firmly bonded onto a polymethyl methacrylate substrate to provide mechanical support and stability throughout the patterning process. Following substrate bonding, a polymer thin film was coated onto the ribbon surface via spin-coating, resulting in a uniform coating with a thickness on the order of several tens of micrometers, as depicted in Fig. 1a1. Subsequently, the polymer layer was microstructured with high precision into an array of well-defined, straight microwires by employing a pulsed laser source with a wavelength of 355 nm. This laser ablation process (Figs. 1a2 and a3) selectively patterned the polymer film, exposing discrete regions of the underlying FeCSi ribbon while preserving the integrity of the microwire design.

Following laser patterning, the exposed FeCSi regions were subjected to a carefully controlled wet chemical etching process, utilizing a specialized etchant solution for a duration of up to ten minutes (Fig. 1a4) [3,8]. This etching step effectively removed the unprotected FeCSi material, thereby defining the microwire geometry. After the etching process was completed, the remaining polymer layer was fully stripped away, revealing the free-standing microwire array (Fig. 1a5). A schematic illustration presenting the fabricated microwires along with their principal dimensional parameters is provided in Fig. 1a5 and a6. Importantly, prior investigations have demonstrated that this fabrication procedure does not induce any detectable changes in the amorphous structure or elemental composition of FeCSi microwires with nominal composition $Fe_{92.9}C_{3.5}Si_{3.6}$, thereby preserving the intrinsic material properties critical for magneto-functional performance [8]. Fig. 1b presents optical microscopy images of the fabricated microwires (Fig. 1b1, b2). The resulting microwires exhibit an approximate width of 80 μm and a length of 9 mm. To facilitate future MI characterizations, the developed microwires were integrated onto a printed circuit board equipped with a pair of subminiature version A connectors to form a complete MI sensor, as shown in Fig. 1b3.

2.2. Experiment

After fabrication, the sensors were first subjected to global magnetic characterization using a vibrating sample magnetometer (VSM, Lakeshore 7400 series) at room temperature. To investigate the impact of DC current, measurements were performed under varying DC currents supplied by a Keithley 236 high-current source through the straight micro-sized conductor configuration.

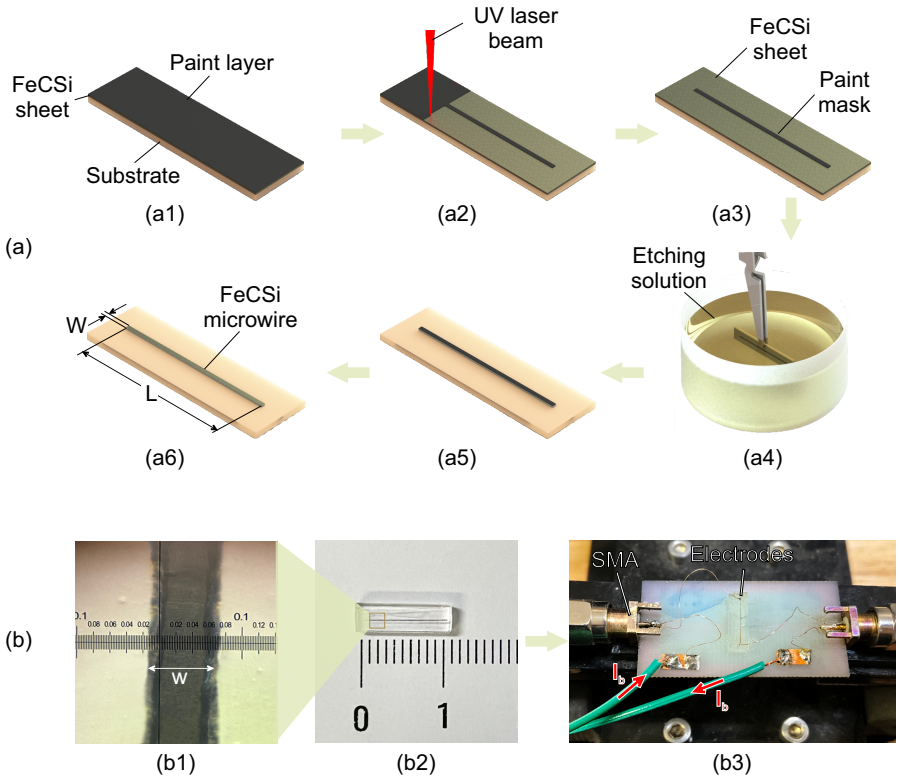

Fig. 1. Overview of the fabrication process for the MI sensor, transforming a continuous FeCSi ribbon into a straight microwire and subsequently integrating it with connectors to complete the sensor assembly. (a) Schematic illustration of the microwire fabrication procedure combining laser ablation and wet chemical etching techniques applied to the continuous FeCSi ribbon; and (b) optical microscope image of the fabricated microwire (b1), photographic image of the microwire after fabrication (b2), microwire mounted and electrically connected to a printed circuit board with electrodes, prepared for MI measurements (b3).

The MI response of the sample was evaluated using a ZNB20 Vector Network Analyzer. Measurements were conducted across variable frequencies up to 3 GHz and under DC magnetic fields of up to 400 Oe, generated by a Helmholtz coil, together with different supplied DC currents.

To assess thermal effects induced by current heating, the temperature increase was characterized with an infrared thermal imaging camera, ensuring high accuracy of $\pm 2^{\circ}$C (Fluke Ti300+, USA). This comprehensive experimental setup enabled precise characterization of the MI response and thermal behavior of the sensors under varying operational conditions, providing critical insights into their performance and optimization for practical applications.

2.3. Computational simulation

MuMax^3 software is utilized in this study to investigate the influence of DC current on the magnetic properties of microwires. This GPU-accelerated micromagnetic simulation tool employs the Finite Difference Method (FDM), dividing the simulation model into uniformly sized cubic

cells [19]. These cell dimensions are 2 nm in each direction and smaller than the exchange length of FeSiC ribbons [20], ensuring validity of the simulation [19]. In the MuMax^3 simulation, the typical magnetic parameters are saturation magnetization of M_s = 1074 kA/m, exchange stiffness constant of A_{ex} = 5 pJ/m [3, 8]. The software solves the Landau-Lifshitz-Gilbert (LLG) equation to compute the magnetization evolution (m), given as:

$$\frac{dm}{dt} = -\gamma m \times H_{eff} + \alpha m \times \frac{dm}{dt}, \tag{1}$$

where γ represents the gyromagnetic ratio, α is the damping parameter, and H_{eff} denotes the effective field. The effective field incorporates contributions from internal fields (magnetostatic (H_d), exchange interaction (H_{exch}), magnetocrystalline anisotropy (H_{anis}), and thermal fluctuation (H_{therm})) and external fields (H_{ext}):

$$H_{eff} = H_{ext} + H_d + H_{exch} + H_{anis} + H_{therm}. \tag{2}$$

To simulate the behavior of microwires under DC current, an additional term h_b is introduced into the external magnetic field. This term represents the circumferential field induced by current flow. The longitudinal axis of the model aligns with the z-axis, while the cross-section lies in the xOy plane. The external field for each FDM cell is expressed as:

$$H_{ext} = (H_x + h_{bx}, H_y + h_{by}, H_z), \tag{3}$$

where h_b = (h_{bx}, h_{bx}, 0). The magnitude of $h_b$scales linearly with r, which is a vector originating from the center of the cross-section to each cell, and its direction is tangential to r.

3. Results and discussion

3.1. Magnetic characterization

The magnetization behavior of the sample under varying external magnetic field orientations is depicted in Fig. 2. When the magnetic field is parallel to the microwire length ($\varphi = 0^\circ$), the magnetization followed in the *M-H* loop rapidly reaches saturation at a relatively low magnetic field strength, approximately 100 Oe. However, as the orientation angle (φ) increases, saturation becomes progressively more difficult to achieve. At $\varphi = 90^\circ$, corresponding to the hard axis (HA), the magnetization process does not reach saturation even under high magnetic fields up to 5000 Oe or 0.5 T. This phenomenon arises from the interplay between Zeemann energy (U_e) under the external magnetic field (H_{ex}) and shape anisotropy energy (U_{sh}), described by [21, 22]:

$$U_e = \frac{\mu_o}{2V} \int \overrightarrow{M}\overrightarrow{H}_{ex} dV, \tag{4}$$

$$U_{sh} = -\frac{\mu_o}{2V} \int NM^2 dV, \tag{5}$$

where V represents the sample volume, M is the magnetization, and N is the demagnetization factor. The value of N, ranging between 0 and 1, depends on the sample's shape, size, and orientation relative to the external field [23]. For a rectangular cross-section microwire with dimensions L, W, and t, N is calculated as 1.8×10^{-3} and 2×10^{-1}, as the external magnetic field is in-plane, parallel and perpendicular to the longitudinal axis of the microwire, respectively. The substantial increase in N explains the dramatic changes observed in the magnetization curves as φ transitions from 0° (easy axis, EA) to 90° (HA). Based on experimental saturation magnetization values of $M_s = 1.34$

T, the external field strengths required for full saturation are extrapolated at approximately 0.25 T for $\varphi = 0^\circ$ and around 2.4 T for $\varphi = 90^\circ$.

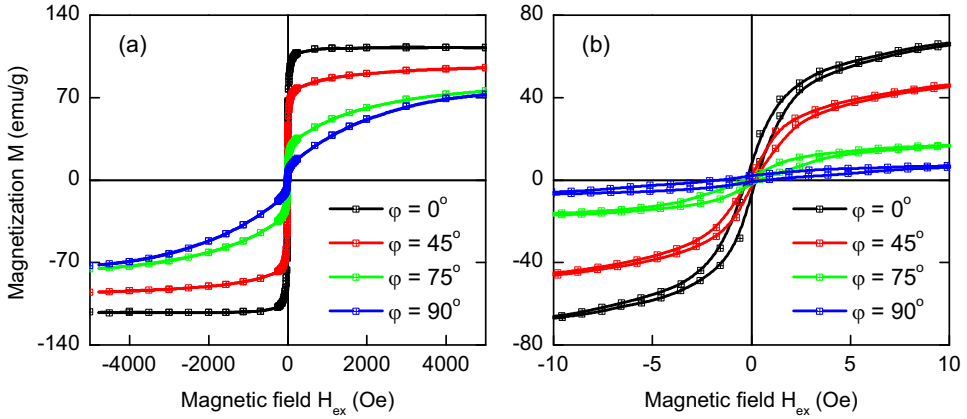

Fig. 2. (Color online) The magnetization dependence of the microwire as a function of the external magnetic field at various φ-angle orientation respect to the microwire's longitudinal axis at high (a) and low (b) magnetic field ranges.

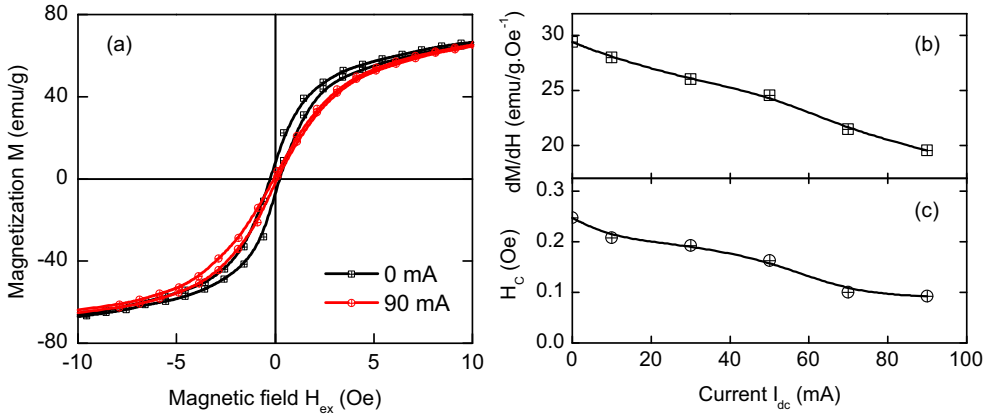

Fig. 3. (Color online) The magnetic hysteresis loop as the magnetic field parallel with the microwire's longitudinal axis under an excited current flow of $I_b = 0$ and 90 mA (a), the magnetic susceptibility and magnetic coercive field plotted as a function of excited current (b).

The influence of electric current on magnetic anisotropy was further investigated by measuring $M(H)$ loops under varying currents ($I_b = 0 - 90$ mA) through the microwire length at $\varphi = 0^\circ$. Results presented in Fig. 3 indicate that increasing current weakens magnetization, highlighting a deterioration in magnetic anisotropy. Magnetic susceptibility, derived from the slope of $M(H)$ loops (Fig. 3b), decreases almost linearly from 29.4 to 19.5 (a reduction of approximately 1.5 times) as I_b increases from 0 to 90 mA. Additionally, coercive field values decrease by a factor of 2.5, from 0.25 Oe to 0.1 Oe (Fig. 3c).

The presence of current generates an internal circumferential bias magnetic field (H_b), creating artificial anisotropy that manifests as helical splines around the microwire [24]. The strength of this anisotropy depends on the distance (r) from the microwire's axis and can be calculated using Ampere's Law [25]:

$$H_b = \frac{rI}{2\pi LW}. \tag{6}$$

This bias field introduces intrinsic magnetostatic energy (U_b), expressed by:

$$U_b = -\frac{\mu_o}{2V}\int \vec{M}\vec{H}_b dV. \tag{7}$$

The interplay between (U_{sh}), (U_b), and (U_e) plays a crucial role in determining the magnetization behavior of microwires. While U_{sh} aligns magnetization along the microwire's length, U_b tends to orient it transversely due to the bias DC current, and U_e aligns the magnetic moment with the applied field. This energy competition is evident in magnetization curves that depend on the external field's strength and direction, as well as the current magnitude flowing through the sample.

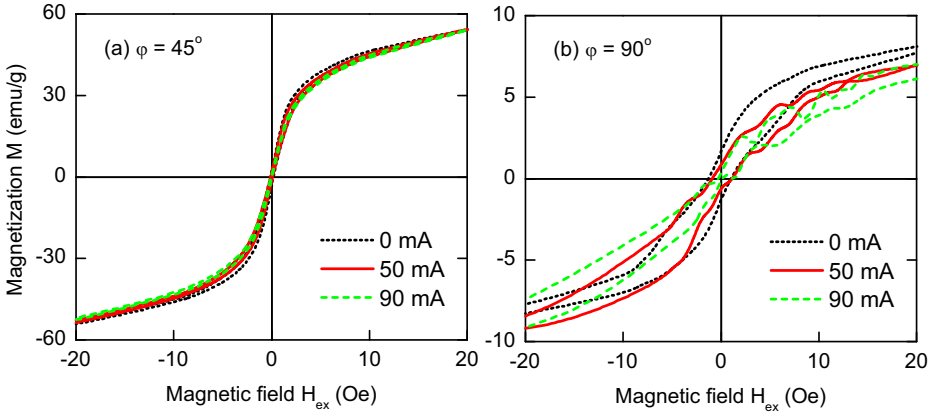

Fig. 4. (Color online) The magnetic hysteresis loops characterized as the magnetic field is parallel with the microwire's longitudinal axis at φ-angles 45° (a) and 90° (b) with various excited current flow from 0 to 90 mA.

To experimentally analyze the U_b, the magnetic energy density was calculated from $M(H)$ loops by $\Psi = \mu_\circ \int_0^M HdM$. The difference in energy density $\Delta\Psi = \Psi(I_b) - \Psi(0)$ between loops at $I_b = 0$ and 90 mA in the low field range (0 to 25 Oe) revealed that U_b contributes approximately 10 % compared to U_e. Although small, this U_b contribution effectively controls the initial anisotropy from longitudinal to transversal axes by using current flow-assisted methods [26]. Similar trends are observed for $M(H)$ loops at different φ-angle orientations, as shown in Fig. 4. Notably, the presence of current perturbs the magnetization at $\varphi = 90°$, potentially due to thermal fluctuations from Joule heating, at which a current I flowing through a resistor with a resistance R in a time interval t:

$$Q = I^2 Rt. \tag{8}$$

To quantify thermal energy contributions, infrared thermal imaging was used to measure temperature increases when current flows through the microwire. Results in Fig. 5 show significant temperature rises only at currents above 50 mA, with a $\Delta T = 20°C$ at 90 mA. This temperature increase is far from the Curie temperature of the FeCSi alloy and becomes significant only when comparable to other magnetostatic energies (U_b and U_e) and anisotropy energy (U_{sh}). Low magnetization, or low magnetic energies, makes thermal energy dominant at high currents, weakening thermal stability in the low-field range along the HA ($\varphi = 90°$). In contrast, $M(H)$ loops at other φ-angles show no fluctuations up to $I_b = 90$ mA, indicating good thermal stability.

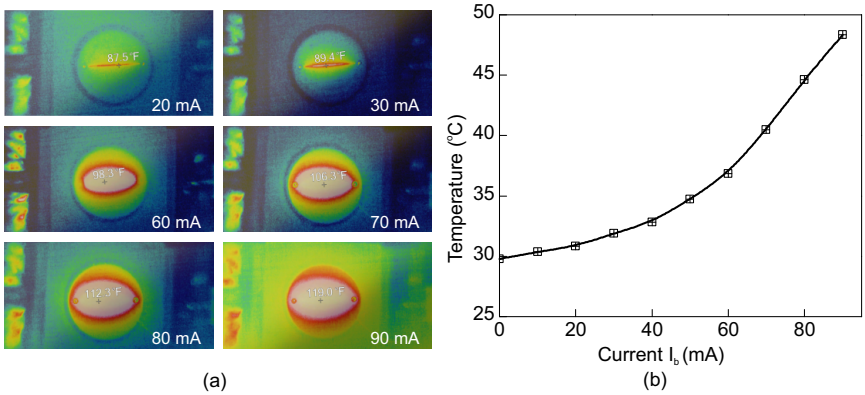

Fig. 5. The infrared thermal images (a) and temperature dependence (b) as a function of excited current flow ranging from 0 to 90 mA.

3.2. Computational micromagnetic simulation

Micromagnetic simulations, as shown in Fig. 6a and 6b, demonstrate good agreement with experimental results for different orientations and DC current flows. As depicted in the 3D magnetization distribution image (Fig. 6c), the coordinate system is defined at the center of the microwire, with the x-, y-, and z-axes corresponding to the microwire's width, thickness, and length, respectively. The magnetic field is aligned parallel to the z-axis, while the current flows along the microwire's length. The magnetization component along the magnetic field direction (M_z) is shown in Fig. 6d1 for $H = 0$ and $I = 0$, revealing the formation of strip domains throughout the sample. These domains, predominantly aligned with the magnetic field, occupy most of the sample volume, a phenomenon attributed to shape anisotropy. This anisotropy establishes the microwire's easy axis along its length, facilitating domain formation.

The magnetic domain structure was further analyzed in the xz-plane at both the middle (Fig. 6d1-d8, top) and top positions (Fig. 6d1-d8, bottom) under varying magnetic fields ($H = 0$ and 50 Oe) and currents (0 to 50 mA). In the absence of current (d1 and d5), there is minimal variation in magnetic domains across xy planes from the center to the top. However, significant differences emerge when current is applied. The magnetization along the z-axis diminishes with increasing distance from the middle plane due to the magnetizing effect of the bias magnetic field generated by the current. This field increases linearly with distance from the center to minimize magnetostatic energy (U_b) and potential energy of magnetic moments (U_e), as described by Eq. (7) and Eq. (4), respectively.

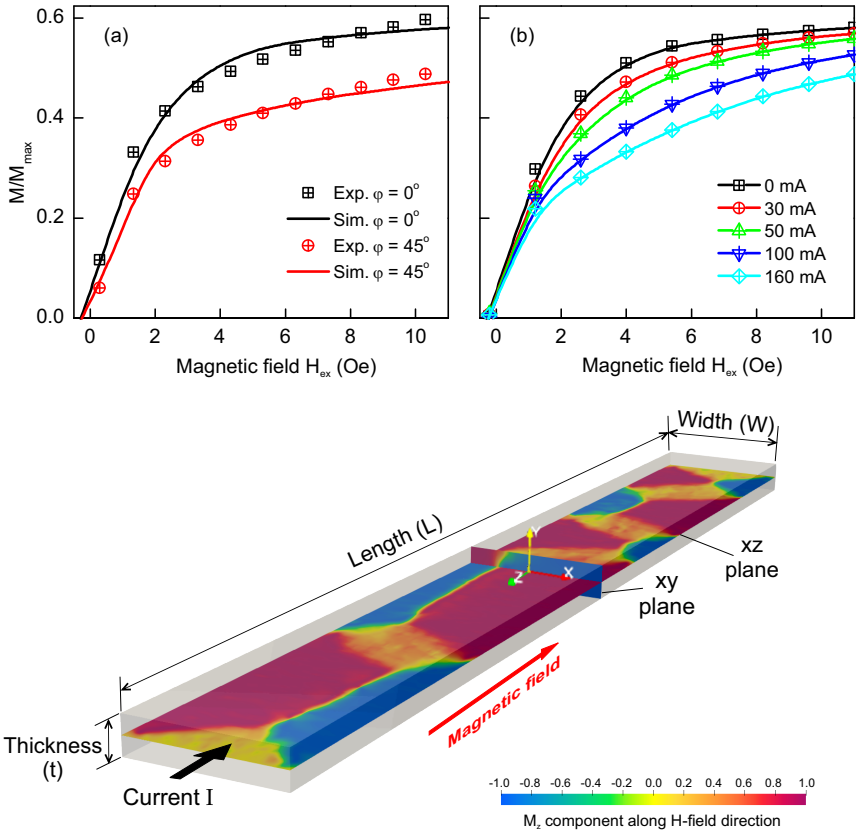

(c) 3D image of magnetization distributions along the magnetic field direction

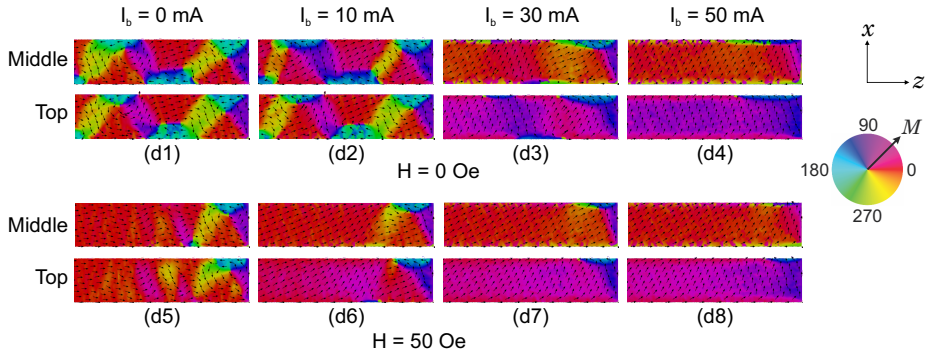

(d) Magnetic moment distribution in xz plane

Fig. 6. The computational magnetic properties estimated from micromagnetic simulation of microwire depending on applied magnetic field at various excited current flows. Parts of normalized hysteresis loops at different φ angles (a), at various excited current flows (b), schematic of 3D magnetization distribution (c), and magnetic moment distribution in xz plane (d).

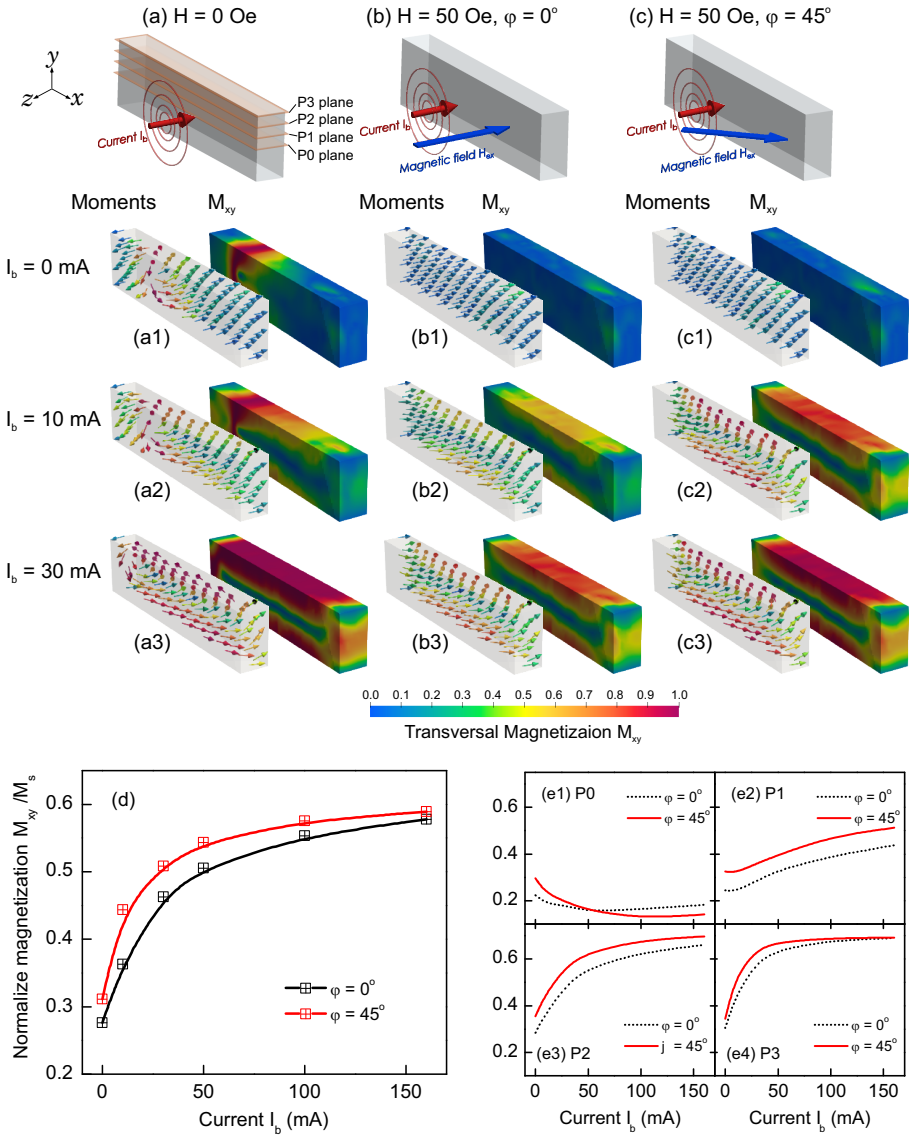

Fig. 7. The computational domain properties of the microwire at different excited current flows: magnetic domain distribution in a block parallel to xy plane in the case of without (a) and with magnetic field applied in $\varphi = 0^\circ$ (b) and $\varphi = 45^\circ$ orientation (c), the dependence of the magnetic transversal component M_{xy} calculated for the entire microwire (d) and in different planes parallel to xz plane (e1-e4) at various excited current flows.

The sharp reduction in M_z near the surface regions correlates with a substantial increase in transverse magnetization (M_{xy}), which is perpendicular to the current flow. Figs. 7a-c illustrates M_{xy} and magnetic moment distributions in the xy-plane. In the absence of an external magnetic field, M_{xy} appears only minimally in domain wall regions (Fig. 7a1) but disappears entirely under

a certain applied field (Fig. 7b1-c1). With current flowing through the microwire, M_{xy} increases significantly, particularly near surface regions (Fig. 7b2,b3), and persists even under external fields up to 50 Oe (Fig. 7c2,c3). The vortex-like structure of magnetic moments around the current is strongest at the surface but weakens towards the center. This behavior agrees with the internal bias field (H_b) generated by electric current, enabling control over anisotropy from longitudinal to transverse axes.

Numerical simulations further analyze M_{xy} responses to current across different sample planes, including P0 (center) and planes closer to the surface (P1–P3). Results in Figs. 7d,e for $\varphi = 0^\circ$ and $\varphi = 45^\circ$ reveal that M_{xy} contributes more prominently at $\varphi = 45^\circ$, especially near surface planes P2 and P3. Saturation occurs at lower currents for $\varphi = 45^\circ$ (30 mA) compared to $\varphi = 0^\circ$ (60 mA). This difference arises from the contributions of horizontal components of external magnetic fields at tilted orientations, reducing required current levels. The findings suggest that optimizing current flow and external field orientation can enhance transverse magnetization responses, thereby improving MI effects. The MI effect is driven by transverse permeability changes induced by alternating currents, particularly near surfaces due to skin depth effects [27,28]. These insights provide a pathway for enhancing MI sensor performance through precise control of magnetization dynamics.

3.3. Magnetoimpedance characterizations

Figure 8a-c presents the magnetic field dependence of MI loops measured under varying bias currents ($I_b = 0$ to 90 mA) and different orientations of the applied magnetic field relative to the microwire axis ($\varphi = 0^\circ$ to 90°). In the absence of any applied current, the MI response demonstrates a pronounced dependence on the angle between the magnetic field and the microwire length. Specifically, the maximum MI ratio of approximately 10.1% is recorded at an intermediate angle of $\varphi = 45^\circ$, which is more than twice the response of 4.8% measured at $\varphi = 0^\circ$, while the MI response is minimal at the perpendicular orientation ($\varphi = 90^\circ$). This angular sensitivity demonstrates the anisotropic magnetic behavior inherent to the microwire geometry and magnetization configuration.

Upon application of a bias current, a substantial enhancement in the MI effect is observed. At $\varphi = 0^\circ$, increasing the current from 0 to 30 mA results in an increase in the MI ratio by a factor of 1.3, from 4.8% to 6.15%. A similar current increment at $\varphi = 45^\circ$ further elevates the MI ratio from 10.1% to a notable 13.5%. Notably, the magnetic field corresponding to the peak MI ratio shifts to lower values, decreasing approximately twofold from 60 Oe to 35 Oe. This shift indicates a modification in the effective magnetic anisotropy and magnetization dynamics caused by the current-induced magnetic field and Joule heating effects.

Thermal characterization, detailed in Fig. 5, reveals that increasing the DC bias current from 0 to 70 mA raises the microwire temperature from approximately 30 °C to 40 °C. Notably, a current increment of 30 mA leads to a temperature rise of around 3°C (from 30 °C to 33 °C), which correlates with an approximate 35% increase in the maximum MI ratio. This strong interplay between temperature and MI response is consistent with previous literature reports, where similar trends in temperature-dependent MI variation have been documented for amorphous and glass-coated microwires. For instance, studies have reported the following temperature-induced MI ratio changes: (i) an increase of approximately 22% for Co-rich glass-coated microwires upon heating from room temperature to 100 °C [29], (ii) a modest rise of 6.6% over a temperature range

of 0 °C to 100 °C for Co–Fe–Si–B amorphous microwires [30], and (iii) a pronounced change of up to 71% in $Co_{70.5}Fe_{4.5}Si_{15}B_{10}$ amorphous microwires as the temperature varies from –23 °C to 127 °C [31]. These comparisons highlight the significant dependence of the MI effect on thermal variations, which must be carefully considered in device design and operation for practical sensing applications.

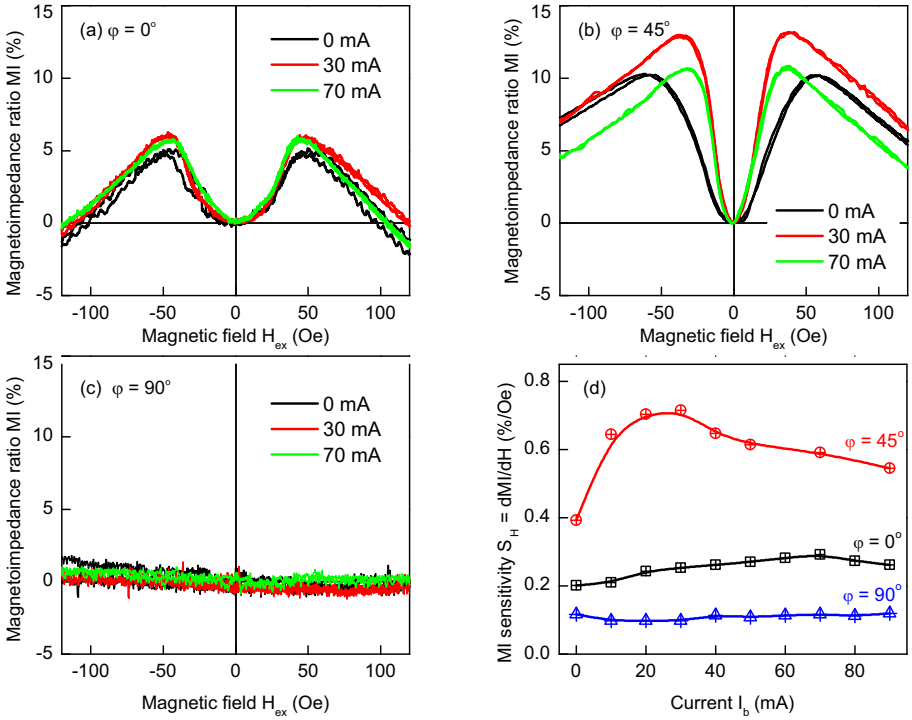

Fig. 8. (Color online) The MI ratio with respect to the applied magnetic field characterized at various current flow and different magnetic field orientation $\varphi = 0°$ (a), 45° (b), 90° (c), and current dependence of MI susceptibility extracted from the MI curves (d)

The MI sensitivity, defined as $S_H = \frac{\Delta MI}{\Delta H}$, is evaluated from the slope of these MI curves. Fig. 8d illustrates the sensitivity as a function of current at different orientation angles. The tilt angle $\varphi = 45°$ is optimal for both the MI ratio and sensitivity. Initially, sensitivity increases rapidly with current from 0.39 %/Oe at $I_b = 0$ mA to a maximum of 0.72 %/Oe at $I_b = 30$ mA, then decreases slowly with further current increases. At $\varphi = 0°$, sensitivity also increases with current, reaching a maximum at 70 mA. These values are in good agreement with the current range for M_{xy} saturated as indicated in the previous discussion.

These findings highlight the advantage of the inclined direction at 45° from the EA axis, where transversal magnetic anisotropy contributes significantly to the high MI response. The addition of a 30 mA DC current enhances this transversal magnetization contribution, leading to improved MI ratios and sensitivities. The experimental results, combined with micromagnetic simulation, demonstrate how controlling transversal magnetic anisotropy via DC current injection explains the observed trends in MI behavior.

4. Conclusions

This study elucidates the role of competing energy mechanisms in enhancing the MI effect in magnetic microwires. The magnetostatic energy generated by the circumferential magnetic field, induced by electric current, significantly enhances the transversal magnetization component, particularly at a 45-degree tilt angle relative to the easy axis. Under these conditions, the MI effect improves by a factor of 1.3, and MI sensitivity increases 3.5-fold compared to scenarios without current and with the field aligned parallel to the microwire length. The improvements in MI performance arise from the interaction between current-induced anisotropy and external field orientation, which modifies the local energy landscape to promote stronger transverse magnetic anisotropy. This optimization enhances both the MI ratio and sensitivity, especially at intermediate tilt angles where longitudinal and transverse components are balanced. By leveraging current-induced anisotropy, this work opens new avenues for designing advanced magnetic sensors with improved resolution and detection capabilities, aligning well with micromagnetic simulation and providing a robust framework for future studies on optimizing MI effects in soft magnetic materials.

Acknowledgments

This work was supported by the National Research Program under the granted Research Project No. DTDL.CN-02/23.

Authors contributions

DT Huong Giang conceived the original idea and supervised the findings of this research. NV Tuan, NK Binh, and LV Lich conducted the computational analyses. VD Lam and HS Hong provided support for the magnetoimpedance measurements. HA Tam and PV Vuong were responsible for manufacturing the microwire patterning and electrical electrodes. DH Hoang established and executed magnetization measurements. The manuscript was collaboratively written by DT Huong Giang and NV Tuan with contributions from all authors.

Conflict of interest

The authors have no conflict of interest to declare.

References

[1] M.-H. Phan and H.-X. Peng, *Giant magnetoimpedance materials: Fundamentals and applications*, Prog. Mater. Sci. **53** (2008) 323.
[2] H. A. Tam, N. V. Tuan, N. T. Ngoc, L. V. Lich, D. V. Hai, M.-H. Phan *et al.*, *Tuning rotational magnetization for high frequency magnetoimpedance in micro-patterned triangle spiral magnetic systems*, J. Sci.: Adv. Mater. Devices **7** (2022) 100514.
[3] N. V. Tuan, H. A. Tam, N. T. Ngoc, V. N. Thuc, N. K. Binh, N. T. P. Thao *et al.*, *High-efficiency microfluidic chip integrated with micro-patterned planar spiral sensors for magnetic nanoparticle detection*, Lab Chip **25** (2025) 2977.
[4] L. Panina and K. Mohri, *Magneto-impedance effect in amorphous wires*, Appl. Phys. Lett. **65** (1994) 1189.
[5] E. Harrison, G. Turney and H. Rowe, *Electrical properties of wires of high permeability*, Nature **135** (1935) 961.
[6] E. Harrison, G. Turney, H. Rowe and H. Gollop, *The electrical properties of high permeability wires carrying alternating current*, Proc. R. Soc. Lond. A **157** (1936) 451.
[7] C. Kittel, *Theory of the dispersion of magnetic permeability in ferromagnetic materials at microwave frequencies*, Phys. Rev. **70** (1946) 281.

[8] V. N. Thuc, H. A. Tam, D. T. H. Giang, N. H. Duc, N. T. Ngoc, V. T. N. Khanh *et al.*, *Hierarchical geometric designs for fe-based amorphous materials with tunable soft magnetic properties*, J. Alloys Compd. **895** (2022) 162628.

[9] T. Nguyen-Van, V. N. Thuc, N. T. Ngoc, H. A. Tam, N. H. Duc, V. T. N. Khanh *et al.*, *Programmable magnetic properties in artificially designed multiferroic composite with giant magnetoelectric coupling*, J. Alloys Compd. **1022** (2025) 179840.

[10] M. Ipatov, V. Zhukova, J. Gonzalez and A. Zhukov, *Manipulating the magnetoimpedance by dc bias current in amorphous microwire*, J. Magn. Magn. Mater. **324** (2012) 4078.

[11] N. Buznikov, A. Antonov and A. Granovsky, *Asymmetric magnetoimpedance in amorphous microwires due to bias current: Effect of torsional stress*, J. Magn. Magn. Mater. **355** (2014) 289.

[12] R. González-Martínez, U. de La Torre, A. Ebel, J. Lacaze and J. Sertucha, *Effects of high silicon contents on graphite morphology and room temperature mechanical properties of as-cast ferritic ductile cast irons. part ii-mechanical properties*, Mater. Sci. Eng. A **712** (2018) 803.

[13] H. Kikuchi, H. Nakamura and C. Sumida, *Influence of direct dc bias current on stepped magnetoimpedance profile and changes in domain structure*, Int. J. Appl. Electromagn. Mech. **59** (2019) 123.

[14] V. Zhukova, J. M. Blanco, M. Ipatov, M. Churyukanova, S. Taskaev and A. Zhukov, *Tailoring of magnetoimpedance effect and magnetic softness of fe-rich glass-coated microwires by stress-annealing*, Sci. Rep. **8** (2018) 3202.

[15] N. Usov, A. Antonov and A. Lagar'kov, *Theory of giant magneto-impedance effect in amorphous wires with different types of magnetic anisotropy*, J. Magn. Magn. Mater. **185** (1998) 159.

[16] L. Kraus, *Theory of giant magneto-impedance in the planar conductor with uniaxial magnetic anisotropy*, J. Magn. Magn. Mater. **195** (1999) 764.

[17] A. Chizhik, J. Gonzalez, A. Zhukov and P. Gawronski, *Review of helical magnetic structures in magnetic microwires*, Chemosensors **10** (2022) 291.

[18] Q. Wang, Y. Zeng, K. Yuan, Q. Zeng, P. Gu, X. Xu *et al.*, "Ultra-efficient magnetism modulation in a weyl ferromagnet by current-assisted domain wall motion." arXiv preprint arXiv:2011.08391, 2020.

[19] A. Vansteenkiste, J. Leliaert, M. Dvornik, M. Helsen, F. Garcia-Sanchez and B. V. Waeyenberge, *The design and verification of mumax3*, AIP Adv. **4** (2014) .

[20] J. M. Coey, *Magnetism and Magnetic Materials*. Cambridge University Press, 2010.

[21] D. J. Dunlop and Ö. Özdemir, *Rock Magnetism: Fundamentals and Frontiers*, no. 3. Cambridge University Press, 1997, 10.1017/CBO9780511612794.

[22] B. M. Moskowitz, M. J. Jackson and V. W. Chandler, *Geophysical properties of the near surface earth: Magnetic*, in *Treatise on Geophysics*, pp. 139–174, Elsevier, (2015), DOI.

[23] A. Aharoni, *Demagnetizing factors for rectangular ferromagnetic prisms*, J. Appl. Phys. **83** (1998) 3432.

[24] M. Vazquez and A. Hernando, *A soft magnetic wire for sensor applications*, J. Phys. D: Appl. Phys. **29** (1996) 939.

[25] D. Owen, *An apparatus for studying the laws of the magnetic field due to an electric current in a long straight conductor*, Br. J. Appl. Phys. **2** (1951) 5.

[26] O. Tikhomirov, *On the control of magnetostatic stray fields using electric current*, J. Surf. Investig. X-ray Synchrotron Neutron Tech. **17** (2023) 556.

[27] P. Delooze, L. Panina, D. Mapps, K. Ueno and H. Sano, *Effect of transverse magnetic field on thin-film magneto impedance and application to magnetic recording*, J. Magn. Magn. Mater. **272** (2004) 2266.

[28] A. Chizhik, V. Vega, A. E.-M. A. Mohamed, V. M. Prida, T. Sánchez, B. Hernando *et al.*, *Surface magnetic properties and giant magnetoimpedance effect in co-based amorphous ribbons*, Intermetallics **86** (2017) 15.

[29] A. Gonzalez, I. Skorvanek, M. Jakubcin, V. Zhukova and A. Zhukov, *Impact of elevated temperature on the giant magnetoimpedance effect in co-rich glass-coated microwires*, Scr. Mater. **266** (2025) 116794.

[30] J. Nabias, A. Asfour and J.-P. Yonnet, *Temperature dependence of giant magnetoimpedance in amorphous microwires for sensor application*, IEEE Trans. Magn. **53** (2016) 1.

[31] J. Santos, R. Varga, B. Hernando and A. Zhukov, *Enhancement of gmi effect in magnetic microwires through the relative temperature dependence of magnetization and anisotropy*, J. Magn. Magn. Mater. **321** (2009) 3875.